# Quantum Simulation of Galton Machines Using Mid-Circuit Measurement and Reuse

Arthur G. Rattew, Yue Sun, Pierre Minssen, and Marco Pistoia JPMorgan Chase & Co., New York, NY, 10017

The efficient preparation of input distributions is particularly important for a wide range of quantum algorithms, such as those for amplitude estimation [1], option pricing [2], principal-component analysis [3], matrix inversion [4], and machine learning [5–7], which all offer the potential for quantum advantage so long as their initial distributions may be generated without introducing computational bottlenecks. We propose a novel quantum algorithm for the general approximate simulation of Galton machines with polynomial depth and bounded error, obtaining exponential quantum advantage over the corresponding classical algorithm. We prove that the proposed procedure may be directly used to efficiently load normal distributions into quantum registers. To the best of our knowledge, our work is the first to leverage the power of Mid-Circuit Measurement and Reuse (MCMR) [8], in a way that is broadly applicable to a range of state-preparation problems. Specifically, our algorithm employs a repeat-until-success scheme, and only requires a constant-bounded number of repetitions in expectation. In the experiments presented, the use of MCMR enables up to a 862.6× reduction in required qubits. Furthermore, the algorithm is provably resistant to both phase-flip and bit-flip errors, leading to a first-of-its-kind empirical demonstration on real quantum hardware, the MCMR-enabled Honeywell System Model H0.

Constructing an arbitrary quantum state necessitates exponential-depth circuits [9]. As a result, any efficient state preparation technique must either be approximate in nature, or exploit information specific to the distribution being generated. Moreover, the quantum computers of the foreseeable future belong to the class of Noisy Intermediate-Scale Quantum (NISQ) hardware, characterized by small qubit counts, limited two-qubit gate fidelity, and short coherence times [10]. As a result, for an algorithm to offer quantum advantage in the near future, it is even more important that state-generation procedures use as shallow circuits with as few ancillary qubits as possible, and produce high-fidelity states even in the presence of low gate-execution fidelity.

Initially proposed by Lloyd and Weedbrook in

2018 for the purpose of generating quantum states, quantum generative adversarial networks (QGANs) employ two agents: a generator and a discrimina-The generator is tasked with producing the desired distribution, which is then evaluated by the discriminator [11]. Numerous papers have since built upon this work, demonstrating QGANs on real quantum processors, and extending QGANs for both classical sampling as well as for loading coherent quantum states [12, 13]. Similarly, it is conceivable that algorithms originally proposed for quantum variational minimization, such as the Variational Quantum Eigensolver (VQE) [14], ADAPT-VQE [15] and Evolutionary VQE (EVQE) [16], could also be used to produce distributions by substituting the expectation-value-based cost function with one measuring the cross-entropy of the output and target distributions. It may also be possible to use these variational algorithms to load a distribution generating a given a data set by defining the cost function as the difference of squares between the input samples and the corresponding measured probabilities. However, as such a procedure relies on obtaining precise measurements of specific state amplitudes, it would have exponential complexity, at best, scaling as  $\mathcal{O}(\sqrt{N})$  thereby still allowing polynomial quantum advantage (noting the intrinsic challenges in providing rigorous error bounds and asymptotic scaling proofs for variational algorithms).

In the creation of exact distributions, or those motivated analytically, a wide range of approaches have been explored. Grover and Rudolph published a procedure for generating efficiently integrable (e.g., log-concave) probability-density functions [17]. While there are some conflicting opinions regarding the theoretical asymptotic efficiency of the described procedure [1, 18]), all agree that this work does not offer an approach that is efficiently realizable in practice on extant NISQ hardware. Kitaev and Webb built upon the aforementioned work by Grover and Rudolph, describing a method of generating multivariate normal distributions through resampling [19], similar to the qubit-scaling procedure we present in this paper, but fundamentally different in a way that causes their approach to rapidly accumulate error. Moreover, resampling only allows for the creation of Gaussian distributions with small variances, and requires the use of multiple ancillary qubits, limiting its practicality in the NISQ era.

Our approach has no such limitations. Häner et al. presented a number of quantum circuits with polynomial depth, implementing commonly encountered functions through piece-wise polynomial approximations [20]. Nevertheless, this approach comes with a significant overhead in both required ancillary qubits, and resulting circuit depths [1]. Moreover, we do not expect this approach to efficiently implement a range of functions, such as the exponential function (and thus normal distributions), as the piece-wise polynomial approach would require an infeasible number of pieces to create accurate models on near-term hardware.

Non-unitary transformations may enable distributions to be obtained more efficiently [21, 22]. Two common ways to implement non-unitary transformations are (1) scaling to higher dimensional spaces through the use of ancillary qubits [20]), and (2) introducing non-linearities by performing partial measurements throughout the coherent execution of a circuit. The use of an asymptotic number of ancillary gubits is not desirable for the purpose of introducing non-unitary transformations, as qubit counts are limited in the NISQ era. As such, we believe it is preferable to use Mid-Circuit Measurement and Reuse (MCMR) [8]. In the context of this work, the MCMR-free approach requires a number of ancillas that scales asymptotically in the variance of the target distribution being generated. As a result, in the experiments performed, the MCMR-based solution we propose uses up to  $862.6 \times$  fewer total qubits and  $8617 \times$  fewer ancillary qubits than its MCMR-free counterpart, thereby making it a more usable statepreparation procedure in the NISQ era.

Repeat-until-success (RUS) paradigms are often used by approaches that introduce non-linearities through the use of mid-circuit partial measurements [23]. In these methodologies, ancillary flag qubits are entangled with primary data registers, and the flags are then measured to determine if a particular operation was applied successfully. If the operation was not applied successfully, it may be possible to apply an operation conditioned on the classical measurement to then obtain the desired output. Alternatively, the circuit may simply be re-executed until the desired transformation is obtained. Guerreschi observes that RUS approaches have been used in applications such as implementing quantum neurons with non-linear activation functions [24, 25], and in the synthesis of arbitrary single-qubit rotations [26]. Moreover, RUS has been applied to a number of quantum arithmetic problems [27]. Our work appears to be the first demonstration of RUS in a state-preparation algorithm.

In summary, this work offers five primary contributions.

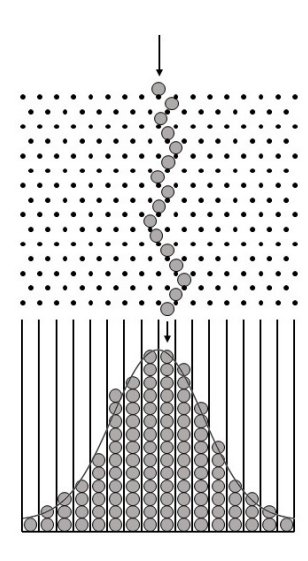


FIG. 1. Galton Machine Visualization. Visual demonstration of a Galton machine generating a normal distribution. Figure adapted from *Option Pricing and Volatility*, by Sheldon Natenberg [28].

- 1. An algorithm for both the exact and approximate simulation of Galton machines, the latter of which runs with  $\mathcal{O}(n^2)$  circuit depth (with n being the number of qubits in the output quantum register) and requires only a single ancilla, or with  $\mathcal{O}(n\log n)$  circuit depth and  $\mathcal{O}(n)$  ancilla qubits.
- 2. The efficient generation of normal distributions in quantum registers, with the only source of error (from the central limit theorem approximation) vanishing exponentially in the number of qubits.
- 3. The first widely applicable state-preparation algorithm to utilize MCMR on real hardware. Specifically, the algorithm uses a RUS scheme combined with MCMR, with an  $\mathcal{O}(1)$  expected rate of success.
- 4. Theoretical error detection and mitigation using only one ancillary qubit, validated by experiments on real quantum hardware.
- 5. A demonstration of the potential of MCMR to enable existing qubit resources to be used asymptotically more efficiently in the introduction of non-unitary transformations. This property is particularly important when working on today's NISQ computers.

#### I. THE ALGORITHM

Our algorithm receives as its input three parameters,  $\hat{\mu}$ ,  $\hat{\sigma}^2$  and l, where  $\hat{\mu}$  and  $\hat{\sigma}^2$  specify the normal distribution  $\mathcal{N}(\hat{\mu}, \hat{\sigma}^2)$ , and l gives the width of the interval under consideration such that the domain is given by  $[\mu - \frac{l}{2}, \mu + \frac{l}{2}]$ . The algorithm aims to produce a quantum state  $|\psi\rangle$  such that

$$|\langle x|\psi\rangle|^2 = \frac{1}{\sqrt{2\pi\hat{\sigma}^2}} \int_x^{x+\Delta x} \exp\left[-\frac{(x'-\hat{\mu})^2}{2\hat{\sigma}^2}\right] dx',$$

where for an n-qubit system,  $\Delta x = l/N$ , with  $N = 2^n$ . As quantum computers operate on discrete state spaces, we will label the set of N basis states with  $\{|x\rangle\}_x$ . Moreover, we will assume that  $\mu$  and  $\sigma^2$  are in units corresponding to the integer-valued basis states, while  $\hat{\mu}$  and  $\hat{\sigma}^2$  are in units corresponding to the input domain. As such, we have that  $\hat{\mu} = \frac{l}{N}\mu$  and  $\hat{\sigma}^2 = \frac{l^2}{N^2}\sigma^2$ . First, we observe that the transition dynamics of

First, we observe that the transition dynamics of a single row in a Galton machine may be described by the transition matrix  $\mathcal{H}$  defined as (up to a normalization factor),

$$\mathcal{H}|x\rangle = |x-1\rangle + |x+1\rangle. \tag{1}$$

Therefore, we may simulate the transition dynamics of a Galton machine with t rows by computing  $\mathcal{H}^t | \psi_i \rangle$  for some starting basis state  $| \psi_i \rangle$  (corresponding to the mean of the distribution produced with  $\mathcal{H}$  as defined in Equation 1). For a more comprehensive overview of the intuition behind these algorithms, see Supplementary Information (SI) 1.

Throughout the remainder of this document, unless we explicitly state otherwise, we assume that our distributions are in terms of the amplitudes of quantum states rather than their probabilities. As shown in SI 2,  $\hat{\sigma}^2 = \frac{l^2}{N^2} \sigma^2 = \frac{l^2}{4N^2} t$ , and so the number of iterations (t) required to obtain a normal distribution with variance corresponding to  $\hat{\sigma}^2$  is given by,

$$\implies t = \frac{4N^2}{l^2}\hat{\sigma}^2. \tag{2}$$

Equation 2 may appear to suggest that to obtain a distribution on n qubits corresponding to a variance  $\hat{\sigma}^2$ , a number of applications of  $\mathcal{H}$  scaling with  $O(2^{2n})$  would be required. This would be problematic, as even if each application of  $\mathcal{H}$  could be implemented in polynomial depth (as we later show, it can) the overall circuit would necessitate exponential depth. Fortunately, as we show in SI 9, it is possible to avoid this exponential blowup by loading a low-resolution version of the distribution on some small constant number of qubits to get the overall "shape" of the distribution, and then by iteratively adding a

least-significant qubit in the  $|+\rangle$  state to transfer the distribution onto a state-space of twice the size (with the mapping  $|x\rangle \rightarrow |2x\rangle + |2x+1\rangle$ , ensuring that adjacent states in the larger Hilbert space share the amplitude of the state in the previous Hilbert space) and applying a polynomial number of correction iterations. To clarify, the mapping  $|x\rangle \rightarrow |2x\rangle + |2x+1\rangle$ is simply performed by adding a qubit, initialized in the state  $|+\rangle$  as the least-significant qubit. Moreover, the correction iterations may simply be implemented by applying  $\mathcal{H}$  without any modifications. While this again directly follows from the central limit theorem, some care must be taken in balancing the number of iterations of  $\mathcal{H}$  that are applied at each qubit count in order to obtain the user-specified variance. The correctness of this procedure, as well as the analysis of the variance as a function of the number of correction iterations, is provided in SI 9. Furthermore, the error in this qubit-scaling approximation may be entirely corrected, meaning that no additional error is introduced by this optimization.

To ensure the efficiency of this procedure, it is essential that  $\mathcal{H}$  be implementable with a polynomialdepth circuit. We have explored a number of approaches, which may be broken into two high-level categories: MCMR-based and MCMR-free. The MCMR-based approach requires only a single ancillary qubit to produce the desired distribution at the cost of requiring a constant-bounded number of expected circuit evaluations, as proven in SI 11. The circuit for the MCMR-based approach is derived and presented in SI 3. The MCMR-free approach requires a number of ancilla qubits scaling linearly in the number of applications of  $\mathcal{H}$  required. This approach is also briefly discussed in SI 3, and is discussed in more detail in SI 5. The complexity of  $\mathcal{H}$  is simply the complexity of the adder gate implementation used. A number of possible implementations for the adder gate are discussed in SI 6, but in summary, this work uses a QFT adder which requires  $\mathcal{O}(n)$  depth (if already in Fourier space), and no additional ancilla gubits. Alternatively, the adder may be implemented with  $\mathcal{O}(n \log n)$  depth if  $\mathcal{O}(n)$  ancilla qubits are available.

Finally, the primary variant of the algorithm, the MCMR-based approach, has provable resistance to hardware errors by virtue of the formulation of  $\mathcal{H}$ . This property is discussed in detail in SI 10, and follows from the probability of the ancilla qubit collapsing to the  $|1\rangle$  state in each application of  $\mathcal{H}$ . In summary, the  $|0\rangle$  and  $|1\rangle$  ancilla states are used to produce a non-unitary transformation in the main register. When the  $|0\rangle$  ancilla state is measured, it is known that the operation was applied successfully. Of essence to the efficiency of this procedure is that the probability of measuring the  $|1\rangle$  state

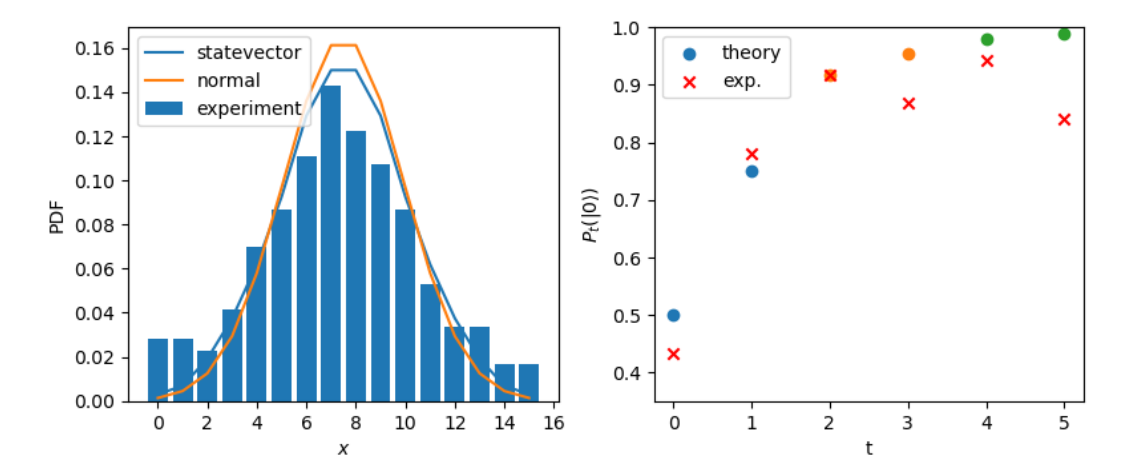


FIG. 2. Samples Drawn from a 5-Qubit Implementation of the Algorithm on the Honeywell System Model H0. In this experiment, the algorithm is configured with  $n_1 = 2$ ,  $n_2 = 3$ ,  $n_3 = 4$ , and  $t_1 = t_2 = t_3 = 2$ . The distribution is then loaded into a quantum register using the proposed algorithm's MCMR variant, and then samples are drawn from the output. Thus, a total of 5 qubits are used in the experiment. The resulting circuit has 75 U1 gates, 60 CX gates, 22 U2 gates, and 10 measurements. A total of 2500 samples are taken, of which only 532 are kept in the algorithm's post-selection process. The left panel presents the post-selected results from the hardware-execution (bar-plot), the ideal statevector distribution (blue line), and the corresponding Gaussian distribution (orange line). Both plots are only assigned values directly on the integer grid points. The panel on the right compares the experimental and theoretical probabilities of obtaining the  $|0\rangle$  state on the ancilla at the  $t^{th}$  iteration, given that all preceding iterations yielded  $|0\rangle$  ancillary measurements. The colors of the circles indicate different qubit scaling stages in the algorithm  $(n_1$  - blue,  $n_2$  - orange,  $n_3$  - green).

decays exponentially in the number of iterations applied. The amplitudes produced on the  $|1\rangle$  state cancel near-optimally, and so if any hardware errors occur, with limited exceptions, they reduce the amount of destructive interference, thus increasing the probability of measuring the ancilla in the  $|1\rangle$  state, and thereby increasing the probability of discarding the error-affected execution. This discussion is treated more rigorously in the aforementioned entry in SI 10.

All together, we have shown how to exactly and approximately simulate Galton machines on quantum computers. The approximate approach requires a polynomial circuit depth and a constant number of expected circuit executions, and can efficiently load a normal distribution with arbitrary variance onto a quantum register – all with provable resistance to hardware noise.

## II. EXPERIMENTAL DEMONSTRATIONS

In this section, we first present and analyze the results from running the MCMR version of the algorithm on the Honeywell System Model H0 [8], and then present the results comparing various variants of the algorithm in numerical simulations.

# A. Quantum Hardware Experiment

The results from the hardware experiment are presented in Figure 2, with the configuration described in the corresponding caption. We use an optimized version of the MCMR-based qubit-scaling algorithm, as presented in SI 4. A total of 2500 samples were taken in this experiment, among which 532 occurred with all of the ancillary measurements yielding the  $|0\rangle$  state. This corresponds to a post-selection rate of 21.28%. In contrast, theoretical calculations indicate that performing this experiment in noiseless simulation would result in a post-selection rate of  $\approx 31.86\%$ . Therefore, there is approximately a 10% deviation from the theoretical prediction and the experimental observations. In the right panel of Figure 2, the y-axis shows the selection rate at the measurement of the  $t^{th}$  application of  $\mathcal{H}$ . The selection rate at t is defined as the probability of measuring a  $|0\rangle$  at that specific iteration given that all prior measurements in the same experiment yielded  $|0\rangle$ . In general, the selection rates observed on the ancillary qubit match the theoretical predictions, especially for the first three applications of  $\mathcal{H}$ , with the relatively small deviations well explained by the intrinsic stochastic variation given the limited quantity of samples collected. After the third application of  $\mathcal{H}$ , the theoretical results and the experimental

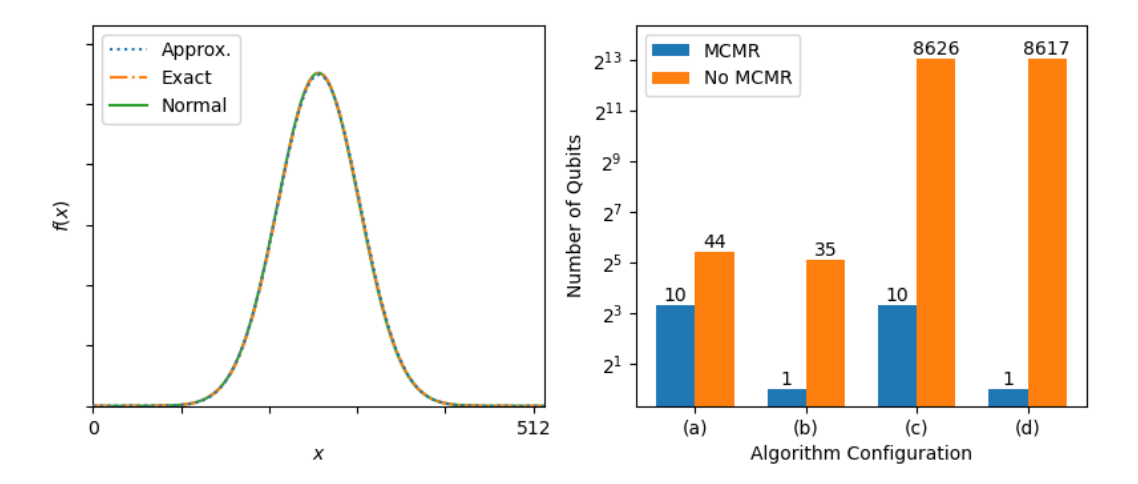


FIG. 3. Simulated Experiment Comparing the MCMR-based and MCMR-free Approaches for the Exact and Approximate Galton Simulators. The left panel of this figure displays the results obtained in theoretical simulation for the approximate Galton simulator with  $n_1 = 5$  scaling up to  $n_5 = 9$ , and with  $t_1 = 32$  and  $t_2 = t_3 = t_4 = t_5 = 4$ . The exact Galton simulator was executed using n = 9 qubits, and with an equivalent effective iteration count of t = 8617. The normal distribution shown is produced by computing the variance and mean corresponding to t = 8617, assuming that t = N. The panel on the right shows the total number of qubits and the number of ancillary qubits required to execute each configuration of the algorithm. The bars labelled t = 1000 represent the total qubit counts for the approximate algorithm, the bars labelled t = 1000 represent the total qubit counts required for the exact algorithm, and the bars labelled t = 1000 represent the ancillary qubit counts required for the exact algorithm.

results start to differ more significantly, insofar as the experimental results reject more samples than error-free analysis predicts. With each application of  $\mathcal{H}$ , additional CX gates are executed, increasing the probability of an error occurring. As predicted in SI 10 as the probability of obtaining an error increases, the probability of discarding a circuit execution also increases, thus explaining the deviations observed. A similar argument also explains the 10% experimental deviation from the theoretical prediction for the total number of shots kept. Indeed, this experimental deviation from the theoretical prediction supports the claim of the algorithm being noise resistant.

# B. Simulated Experiment

In Figure 3, we compare the exact and approximate Galton simulators, along with their MCMR-based and MCMR-free variants. We first configure the approximate Galton simulator with  $n_1 = 5$  scaling up to  $n_5 = 9$ , and with  $t_1 = 32$  and  $t_2 = t_3 = t_4 = t_5 = 4$ . We run the exact Galton simulator on n = 9 qubits, and with an iteration count of t = 8617. Both simulators are expected to generate a distribution with  $\sigma^2 = 2154.25$  and  $\mu = 256$ . Results from the simulators are plotted along with a normal distribution with the same mean and vari-

ance. All of the produced curves are shown on top of each other, demonstrating the effective equivalence of all three distributions. The panel on the right of Figure 3 shows the number of ancillary and total qubits required for the exact and approximate simulators with and without MCMR. The exact simulator requires  $8617\times$  fewer ancillary qubits and  $862.6\times$  fewer total qubits when using MCMR. The approximate simulator requires  $35\times$  fewer ancillary qubits, and  $4.4\times$  fewer total qubits. Clearly, these reductions in required qubit resources will only *increase* as the variance of the desired distribution increases.

#### III. CONCLUSION

This work presents a novel quantum algorithm for both the exact and approximate simulation of Galton machines, the latter of which runs with  $\mathcal{O}(n^2)$  circuit depth (with n being the number of qubits in the output quantum register) and a single ancilla, or with  $\mathcal{O}(n\log n)$  circuit depth and  $\mathcal{O}(n)$  ancilla qubits. The algorithm uses a repeat-until-success scheme combined with MCMR technology, with an  $\mathcal{O}(1)$  expected rate of success. Moreover, we demonstrate how the approximate Galton simulator may be used to produce normal distributions in quantum registers, with the only source of error (from the central limit theorem approximation) vanishing

exponentially in the number of qubits. In addition, this work also demonstrates the potential of MCMR technology in the NISQ era by highlighting how it can enable existing qubit resources to be used asymptotically more efficiently in the introduction of non-unitary transformations, and by demonstrating how it allows qubit-efficient error detection and error mitigation techniques.

## ACKNOWLEDGMENTS

We would like to thank Austin Gilliam and Constantin Gonciulea (JPMorgan Chase) and Saori Pastore (Washington University in St. Louis) for the

insightful discussions on the material presented in this paper. Special thanks to Tony Uttley, Brian Neyenhuis and the rest of the Honeywell Quantum Solutions team for assisting us on the execution of the experiments on the Honeywell System Model H0.

# **AUTHOR CONTRIBUTIONS**

A.G.R. concieved of the project and designed the proposed algorithms. Y.S., A.G.R., P.M., and M.P. contributed further optimizations to the algorithms, and developed the theory. A.G.R., Y.S., and M.P. implemented the algorithm. All authors contributed to the manuscript.

- [1] Almudena Carrera Vazquez and Stefan Woerner. Efficient state preparation for quantum amplitude estimation. arXiv preprint arXiv:2005.07711, 2020.
- [2] Nikitas Stamatopoulos, Daniel J Egger, Yue Sun, Christa Zoufal, Raban Iten, Ning Shen, and Stefan Woerner. Option pricing using quantum computers. Quantum, 4:291, 2020.
- [3] Seth Lloyd, Masoud Mohseni, and Patrick Rebentrost. Quantum principal component analysis. Nature Physics, 10(9):631–633, 2014.
- [4] Aram W Harrow, Avinatan Hassidim, and Seth Lloyd. Quantum algorithm for linear systems of equations. *Physical review letters*, 103(15):150502, 2009.
- [5] Carlo Ciliberto, Mark Herbster, Alessandro Davide Ialongo, Massimiliano Pontil, Andrea Rocchetto, Simone Severini, and Leonard Wossnig. Quantum machine learning: a classical perspective. Proceedings of the Royal Society A: Mathematical, Physical and Engineering Sciences, 474(2209):20170551, 2018.
- [6] Kosuke Mitarai, Makoto Negoro, Masahiro Kitagawa, and Keisuke Fujii. Quantum circuit learning. *Physical Review A*, 98(3):032309, 2018.
- [7] Patrick Rebentrost, Masoud Mohseni, and Seth Lloyd. Quantum support vector machine for big data classification. *Physical review letters*, 113(13): 130503, 2014.
- [8] JM Pino, JM Dreiling, C Figgatt, JP Gaebler, SA Moses, CH Baldwin, M Foss-Feig, D Hayes, K Mayer, C Ryan-Anderson, et al. Demonstration of the qccd trapped-ion quantum computer architecture. arXiv preprint arXiv:2003.01293, 2020.
- [9] Martin Plesch and Časlav Brukner. Quantumstate preparation with universal gate decompositions. *Physical Review A*, 83(3):032302, 2011.
- [10] John Preskill. Quantum computing in the nisq era and beyond. *Quantum*, 2:79, 2018.
- [11] Zhaoqing Pan, Weijie Yu, Xiaokai Yi, Asifullah Khan, Feng Yuan, and Yuhui Zheng. Recent progress on generative adversarial networks (gans): A survey. IEEE Access, 7:36322–36333, 2019.

- [12] Christa Zoufal, Aurélien Lucchi, and Stefan Woerner. Quantum generative adversarial networks for learning and loading random distributions. npj Quantum Information, 5(1):1–9, 2019.
- [13] Ling Hu, Shu-Hao Wu, Weizhou Cai, Yuwei Ma, Xianghao Mu, Yuan Xu, Haiyan Wang, Yipu Song, Dong-Ling Deng, Chang-Ling Zou, et al. Quantum generative adversarial learning in a superconducting quantum circuit. Science advances, 5(1):eaav2761, 2019.
- [14] Alberto Peruzzo, Jarrod McClean, Peter Shadbolt, Man-Hong Yung, Xiao-Qi Zhou, Peter J Love, Alán Aspuru-Guzik, and Jeremy L O'brien. A variational eigenvalue solver on a photonic quantum processor. Nature communications, 5:4213, 2014.
- [15] Harper R Grimsley, Sophia E Economou, Edwin Barnes, and Nicholas J Mayhall. An adaptive variational algorithm for exact molecular simulations on a quantum computer. *Nature communications*, 10 (1):1–9, 2019.
- [16] Arthur G Rattew, Shaohan Hu, Marco Pistoia, Richard Chen, and Steve Wood. A domain-agnostic, noise-resistant, hardware-efficient evolutionary variational quantum eigensolver. arXiv, pages arXiv– 1910, 2019.
- [17] Lov Grover and Terry Rudolph. Creating superpositions that correspond to efficiently integrable probability distributions. arXiv preprint quantph/0208112, 2002.
- [18] Adam Holmes and AY Matsuura. Efficient quantum circuits for accurate state preparation of smooth, differentiable functions. arXiv preprint arXiv:2005.04351, 2020.
- [19] Alexei Kitaev and William A Webb. Wavefunction preparation and resampling using a quantum computer. arXiv preprint arXiv:0801.0342, 2008.
- [20] Thomas Häner, Martin Roetteler, and Krysta M Svore. Optimizing quantum circuits for arithmetic. arXiv preprint arXiv:1805.12445, 2018.
- [21] Bahram Ahansaz and Abbas Ektesabi. Quantum speedup, non-markovianity and formation of bound

- state. Scientific reports, 9(1):1–12, 2019.
- [22] Viv Kendon and Olivier Maloyer. Optimal computation with non-unitary quantum walks. *Theoretical computer science*, 394(3):187–196, 2008.
- [23] Adam Paetznick and Krysta M Svore. Repeat-untilsuccess: Non-deterministic decomposition of singlequbit unitaries. arXiv preprint arXiv:1311.1074, 2013.
- [24] Yudong Cao, Gian Giacomo Guerreschi, and Alán Aspuru-Guzik. Quantum neuron: an elementary building block for machine learning on quantum computers. arXiv preprint arXiv:1711.11240, 2017.
- [25] Wei Hu. Towards a real quantum neuron. Natural Science, 10(3):99–109, 2018.
- [26] Alex Bocharov, Martin Roetteler, and Krysta M Svore. Efficient synthesis of universal repeat-untilsuccess quantum circuits. *Physical review letters*, 114(8):080502, 2015.
- [27] Nathan Wiebe and Martin Roetteler. Quantum arithmetic and numerical analysis using repeat-until-success circuits. arXiv preprint arXiv:1406.2040, 2014.
- [28] Sheldon Natenberg. Option volatility and pricing: Advanced trading strategies and techniques. McGraw-Hill Education, 2014.

- [29] Sam McArdle, Tyson Jones, Suguru Endo, Ying Li, Simon C Benjamin, and Xiao Yuan. Variational ansatz-based quantum simulation of imaginary time evolution. npj Quantum Information, 5 (1):1-6, 2019.
- [30] Michael A Nielsen and Isaac Chuang. Quantum computation and quantum information, 2002.
- [31] Thomas G Draper. Addition on a quantum computer. arXiv preprint quant-ph/0008033, 2000.
- [32] Thomas G Draper, Samuel A Kutin, Eric M Rains, and Krysta M Svore. A logarithmic-depth quantum carry-lookahead adder. arXiv preprint quantph/0406142, 2004.
- [33] Stephane Beauregard. Circuit for shor's algorithm using 2n+3 qubits, 2002.
- [34] Adriano Barenco, Charles H Bennett, Richard Cleve, David P DiVincenzo, Norman Margolus, Peter Shor, Tycho Sleator, John A Smolin, and Harald Weinfurter. Elementary gates for quantum computation. *Physical review A*, 52(5):3457, 1995.
- [35] Hale F Trotter. On the product of semi-groups of operators. *Proceedings of the American Mathematical Society*, 10(4):545–551, 1959.
- [36] Ying Li and Simon C Benjamin. Efficient variational quantum simulator incorporating active error minimization. *Physical Review X*, 7(2):021050, 2017.

#### SUPPLEMENTARY INFORMATION:

## APPROXIMATE AND EXACT QUANTUM SIMULATION OF GALTON MACHINES

# 1. Motivating the Algorithm

Continuing with the notation introduced in Section I, we now provide the intuition motivating the state generating algorithm. According to the de Moivre-Laplace theorem, a binomial distribution B(t,p) converges to a normal distribution with mean tp and standard deviation  $\sqrt{tp(1-p)}$  as  $t\to\infty$ . This property is exploited by Galton machines, such as the one shown in Figure 1, to generate normal distributions by dropping balls through a sequence of rows, where in each row the falling ball may have its position shifted by either one bin to the left, or one bin to the right. As a result, the transition dynamics of a single row in a Galton machine may be described by the transition matrix  $\mathcal{H}$  defined as (up to a normalization factor)

$$\mathcal{H}|x\rangle = |x-1\rangle + |x+1\rangle$$
.

As previously mentioned, the quality of the approximation of the normal distribution produced by a Galton machine improves as more balls are dropped through the system. Moreover, as our quantum Galton approach simulates an infinite number of balls falling through the system (by virtue of operating on superpositions of "bins"), we avoid this type of error entirely. As a result, combined with the exponential growth in the number of bins in terms of the number of qubits, the distributions we produce are indistinguishable from the target normal distributions (i.e. our only source of error is that incurred by the central limit theorem approximation, and the central limit theorem error vanishes exponentially in the number of qubits, and so our approximation rapidly becomes exact).

It is worth briefly mentioning that we explored another variant of the algorithm simulating  $e^{\mathcal{H}t}$  (instead of  $\mathcal{H}^t$ ) to obtain the desired normal distribution. This approach utilizes Imaginary Time Evolution (ITE) to simulate  $e^{\mathcal{H}t}$ , as proposed by McArdle *et al.* in 2019 [29], and is discussed in greater depth in SI 13.

# 2. Deriving $t - \hat{\sigma}^2$ and $t - \hat{\mu}$ Relationships

Applying  $\mathcal{H}^t$  to some initial state produces a normal distribution (on the amplitudes) equivalent to that produced by a Galton machine with t rows. As such, the mean of the produced distribution is given by  $\mu = \frac{t}{2}$ , while the standard deviation is given by  $\sigma = \frac{1}{2}\sqrt{t}$ . Note that if we wish to obtain a given variance in the probability distribution rather than in the amplitudes, by property of a normal distribution, we may simply produce  $2\times$  the desired probability variance as the amplitude variance. Throughout the remainder of this document, unless we explicitly state otherwise (e.g. by writing a probability mass function explicitly), we assume that our distributions are in terms of the amplitudes of quantum states rather than their probabilities. Then, we may compute the number of applications of  $\mathcal H$  required to obtain a normal distribution with variance corresponding to  $\hat{\sigma}^2$  as follows,

$$\hat{\sigma}^2=\frac{l^2}{N^2}\sigma^2=\frac{l^2}{4N^2}t,$$

$$\implies t = \frac{4N^2}{l^2}\hat{\sigma}^2.$$

# 3. Implementing $\mathcal{H}$ as a Quantum Circuit with Mid-Circuit Measurement and Reuse (MCMR)

In order to make the implementation of  $\mathcal{H}$  as a quantum circuit more straight forward, we will redefine the transition matrix. Instead of performing the transformation  $\mathcal{H}|x\rangle = |x-1\rangle + |x+1\rangle$ , we will now perform the mapping  $\mathcal{H}|x\rangle = |x\rangle + |x+1\rangle$ . In so doing, we must pay additional attention to ensure that the mean of the generated distribution is configured correctly, and in exchange, we reduce the complexity of certain sections of the analysis. First, observe that this transition matrix still generates a normal distribution in the same way as the first matrix, only that instead of alternating between zero amplitude even and odd states with each application of  $\mathcal{H}$ , all states are utilized without the need for the input state to contain a superposition of adjacent states (or without the need of additional ancillary qubits). We will now define an addition operator,  $A_{n+1}^{+1}$ , where the subscript indicates the control qubit, and the superscript indicates the quantity added to each state in the first n-qubit register. For example,  $A_{n+1}^{+1}|x\rangle|1\rangle = |x+1\rangle|1\rangle$ , and  $A_{n+1}^{+1}|x\rangle|0\rangle = |x\rangle|0\rangle$ . We then derive the quantum circuit as follows. First we apply a Hadamard gate, H, on the ancilla qubit,

$$I^{\otimes n} \otimes H |x\rangle |0\rangle = |x\rangle (|0\rangle + |1\rangle).$$

Then we apply the +1 gate on the main register, controlled on the ancilla,

$$A_{n+1}^{+1} |x\rangle (|0\rangle + |1\rangle) = |x,0\rangle + |x+1,1\rangle.$$

Finally, we apply another Hadamard gate on the ancilla,

$$I^{\otimes n} \otimes H(|x,0\rangle + |x+1,1\rangle)$$

$$= |x,0\rangle + |x,1\rangle + |x+1,0\rangle - |x+1,1\rangle$$

$$= (|x\rangle + |x+1\rangle) |0\rangle + (|x\rangle - |x+1\rangle) |1\rangle.$$

We see that upon measuring the ancilla qubit in the  $|0\rangle$  state, the main register will contain the state  $|x\rangle + |x+1\rangle$  as desired. However, if we measure the ancilla in the  $|1\rangle$  state, the main register will be found in the incorrect state  $|x\rangle - |x+1\rangle$ . Initially, methods for correcting this error were explored, however, we realized that  $|x\rangle - |x+1\rangle$  actually represents a pattern of destructive interference that exponentially approaches net zero amplitude as a function of the number of iterations applied. As a result, a single iteration of the circuit implementation of  $\mathcal{H}$  may be produced by following the procedure just described, and by measuring the ancilla qubit, continuing if the desirable ancilla state is measured, and terminating execution if the undesirable state is measured. As will be proved shortly, this procedure requires an increase in the expected number of circuit evaluations growing sub-linearly in the number of iterations performed, and therefore results in a polynomially bounded total number of circuit executions for the algorithm as a

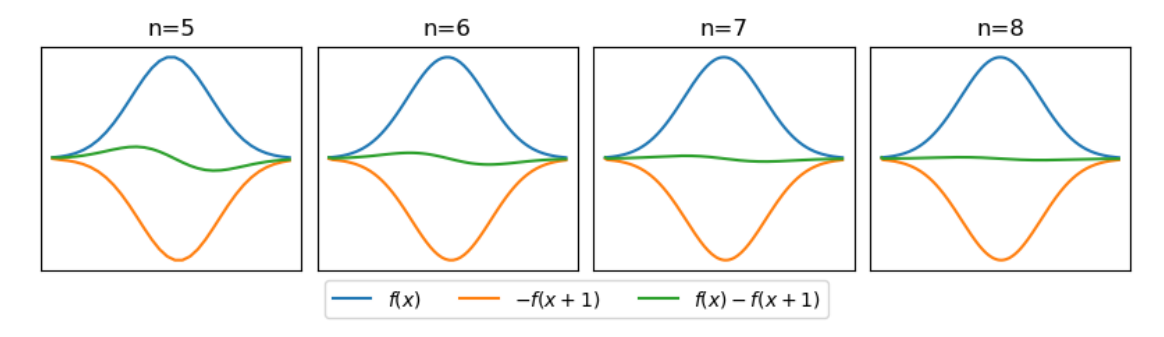


FIG. 4. Amplitude Cancellation Demonstration. This figure demonstrates the interference pattern produced when an initial distribution f(x) is mapped to f(x) - f(x+1) at various qubit counts.

whole. These claims are motivated in SI 3a, and proven in SI 11. In contrast, in the MCMR-free approach, as the single ancilla is not reused subsequently to being measured, a new ancilla qubit must be added for each application of  $\mathcal{H}$ . Each ancilla may be measured at the end of the application of  $\mathcal{H}$ , or by the principle of deferred measurement [30], all added ancillas may be simultaneously measured at the end of the circuit's execution. A more detailed explanation of the MCMR-free approach is presented in SI 5.

#### a. Ancilla |1\rangle State Cancellation Analysis

The implementation of  $\mathcal{H}$  just described relies upon performing a partial measurement on the state,  $(|x\rangle + |x+1\rangle) |0\rangle + (|x\rangle - |x+1\rangle) |1\rangle$ . If the ancilla is measured in the  $|0\rangle$  state, the desired transformation yielding  $|x\rangle + |x+1\rangle$  has been obtained in the main register. If the ancilla is measured in the  $|1\rangle$  state, the undesired state of  $|x\rangle - |x+1\rangle$  is obtained. We claim, and prove in SI 11, that the probability of measuring the  $|1\rangle$  ancillary state rapidly vanishes as a function of the number of applications of  $\mathcal{H}$  performed, and that as a result, we only need to repeat the algorithm's execution a number of times sub-linear in the number of applications of  $\mathcal{H}$  (and in the case of the qubit scaling approach, a constant-bounded number of times). To understand this, it may be more clear to understand an equivalent statement. Given a distribution on n qubits obtained by computing  $\mathcal{H}^t$ , with t computed taking into account n and the input variance, the behavior of the mapping  $|x\rangle \to |x\rangle - |x+1\rangle$  may be similarly expressed in terms of functions of the amplitudes as  $f(x) \to f(x) - f(x + \Delta x)$ , where  $\Delta x = \frac{l}{2^n}$ . As such, given a fixed variance  $\hat{\sigma}^2$ , as we increase the number of qubits, we are exponentially decreasing the relative shift between distributions f(x) and  $-f(x+\Delta x)$ , and so the two distributions rapidly approach f(x) and -f(x), meaning that the interference pattern on the  $|1\rangle$  ancilla state exponentially approaches complete destructive interference as the number of qubits increase. Indeed, in SI 12 we have shown that this cancellation property holds for any continuous function f. This principle is clearly illustrated in Figure 4, where the interference pattern produced rapidly approaches complete destructive interference as the number of qubits increase up to 8.

#### b. Quantum Circuit Implementation of H

Again, the mapping we wish to perform is given by  $\mathcal{H}|x\rangle = |x\rangle + |x+1\rangle$ . To perform such a mapping, we use four components: the QFT, the (Fourier space) adder gate, the Hadamard gate, and mid circuit measurement and reuse. Assuming we are in the Fourier space, (i.e. a QFT has already been performed previously in the circuit),  $\mathcal{H}$  is implemented as shown in Figure 5. As the adder gate may be implemented with O(n) two-qubit gates and depth, one iteration according to  $\mathcal{H}$  is also implemented in linear depth and with linear two-qubit gates. The adder gate and its quantum circuit, along with the corresponding controlled adder gate, is presented in SI 7 and SI 8.

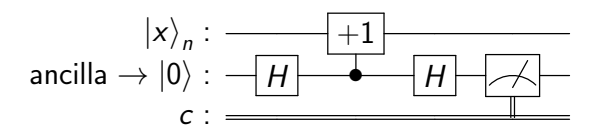


FIG. 5. Quantum circuit implementation of  $\mathcal{H}$ , with the definition  $\mathcal{H}|x\rangle = |x\rangle + |x+1\rangle$  (up to a normalization factor). Note that circuit execution only proceeds if the ancilla is measured in the  $|1\rangle$  state.

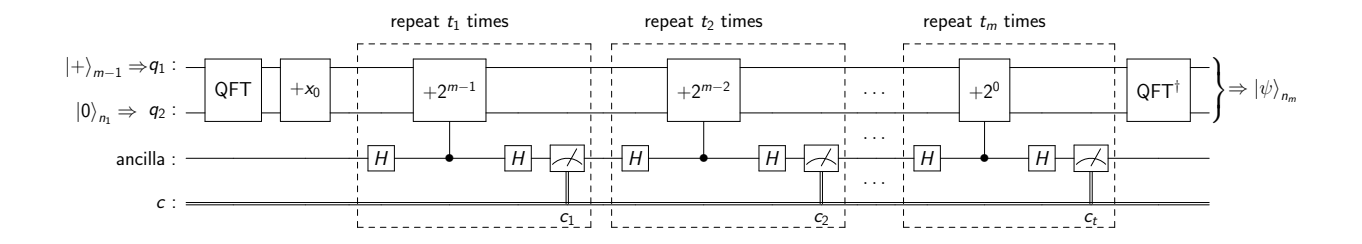


FIG. 6. Quantum circuit implementing the quantum Galton machine with qubit scaling.

# 4. Algorithm Quantum Circuit Implementation

We first present a basic circuit used to implement  $\mathcal{H}^t$ , proceed to give the implementation of the full quantum circuit, including the qubit scaling procedure. The naive circuit (which is used for the exact simulation of Galton machines) uses two quantum registers: one with  $n = n_m$  qubits for the output and the other 1-qubit register as the ancilla. The two registers are initialized in joint state  $|0\rangle_{n+1}$ . We then apply QFT on the n-qubit register to bring the quantum register into Fourier space. Subsequently, we apply  $\mathcal{H}$  which consists of a Hadamard gate on the ancilla qubit, followed by a controlled +1 gate  $(A_j^{+1})$  controlled on the ancilla, a second Hadamard gate on the ancilla, and a measurement on the ancilla. The application of  $\mathcal{H}$  is repeated t times, with the value of t given by Equation 2. In the end, we apply an inverse-QFT on the output register to go back to the real space. The success of the circuit depends on the measurement results on the ancilla qubit. We repeat the circuit until all measurement results come out as 0.

As discussed at the beginning of Section I, the naive implementation without qubit scaling described above would require exponential number of  $\mathcal{H}$  applications, which renders the algorithm inefficient. To address this issue, we use a qubit scaling scheme which significantly reduces the circuit depth with only nominal sacrifices in accuracy. The circuit is illustrated in Figure 6. We start with a small, constant, number of qubits  $n_1$ , and apply  $\mathcal{H}$   $t_1$  times to get close to the desired variance of the distribution. Then we add one qubit to the least significant end in the sate  $|+\rangle$ , and apply  $\mathcal{H}$   $t_2$  times. We repeat the process of adding qubits and applying  $\mathcal{H}$  untill we reach the desired number of qubits  $n_m$ . The values of  $t_1, t_2, \ldots, t_m$  are determined by the scaled variance  $\hat{\sigma}^2$  of the distribution, the formulas of which are given in SI 9. Note that the total number of applications of  $\mathcal{H}$ , i.e.  $\sum_{r=1}^m t_r$  scales as  $O(n_m)$ , as discussed at the beginning of Section I, and in SI 9.

To avoid going back and forth between the real space and the Fourier space when increasing the number of qubits, we perform QFT on the entire  $n_m$  qubit register and inverse-QFT at the very end. Accordingly, the controlled +1 gates in the r-th stage with  $n_r$  qubits would be changed to a controlled +2<sup>m-r</sup> gate on the  $n_m$  qubit register. Note that this still amounts to  $n_r$  controlled-U1 operations in the controlled adder gate, as U1 gates with angles that are multiples of  $2\pi$  amount to the identity gate.

In the case where the mean of the outcome distribution needs to be adjusted, an additional adder gate  $+x_0$  may be added on the  $n_m$ -qubit register in the Fourier space, as shown in Figure 6.

# 5. Implementing $\mathcal{H}$ as a Quantum Circuit without Mid-Circuit Measurement and Reuse (MCMR-free)

We now describe the implementation of the transition matrix  $\mathcal{H}$  defined as  $\mathcal{H}|x\rangle = |x\rangle + |x+1\rangle$  without the use of Mid-Circuit Measurement and Reuse technology. We first perform a derivation similar to that performed in SI 3. Examining one application of  $\mathcal{H}$ ,

$$|x\rangle |+\rangle \xrightarrow{A_{n+1}^{+1}} |x\rangle |0\rangle + |x+1\rangle |1\rangle \xrightarrow{I^{\otimes n} \otimes H} (|x\rangle + |x+1\rangle) |0\rangle + (|x\rangle - |x+1\rangle) |1\rangle.$$

When mid-circuit measurement is used, the preceding final quantum state may simply be measured, as described in a preceding SI entry. However, when MCMR technology is not available, the ancilla cannot be measured until the end of the circuit execution, and so to perform another iteration by  $\mathcal{H}$  we must add another ancillary qubit so as to preserve the state of the first ancilla. In order to reveal some of the properties of this MCMR-free approach, we will now examine the state of the system after performing a second application of  $\mathcal{H}$ . First, we add another ancillary qubit initialized in the  $|+\rangle$  state to obtain,

$$(|x\rangle + |x+1\rangle) |0\rangle |+\rangle + (|x\rangle - |x+1\rangle) |1\rangle |+\rangle.$$

We subsequently apply the adder +1 gate conditioned on the second ancilla,  $A_{n+2}^{+1}$ , to obtain the state,

$$(|x\rangle+|x+1\rangle)|00\rangle+(|x+1\rangle+|x+2\rangle)|01\rangle+(|x\rangle-|x+1\rangle)|10\rangle+(|x+1\rangle-|x+2\rangle)|11\rangle.$$

Simplifying and applying  $I^{\otimes n+1} \otimes H$  then yields,

$$(|x\rangle + 2|x+1\rangle + |x+2\rangle)|00\rangle + (|x\rangle - |x+2\rangle)|01\rangle + (|x\rangle - |x+2\rangle)|10\rangle - (|x\rangle - 2|x+1\rangle + |x+2\rangle)|11\rangle.$$

It now becomes clear that upon adding a new ancillary qubit, and performing the standard operations required to implement an additional iteration according to  $\mathcal{H}$ , that the probability of measuring the  $|1\rangle$  state of any preceding ancilla qubits remains unchanged. As such, the analysis regarding the probability of measuring all ancilla qubits in the  $|0\rangle$  state, and thus of obtaining the correct state in the primary register, follows the same analysis as the MCMR-based version of the algorithm.

## 6. Adder Gate Complexity

All approaches require the implementation of an adder-plus-one gate  $(A^{+1})$ , which can be implemented either with additional ancillary qubits, or with no additional ancillary qubits. When not using ancillary qubits, the adder-plus-one gate may be implemented in Fourier space (requiring a Quantum Fourier Transform (QFT) at the start of the overall circuit, and an inverse-QFT at the end) resulting in  $\mathcal{O}(n)$  CX gates per application of  $\mathcal{H}$  [31]. Alternatively, without additional ancillas, the adder-plus-one gate may be implemented with  $\mathcal{O}(n^2)$  CX gates per application of  $\mathcal{H}$ . As a result, we use the QFT adder approach throughout this document, resulting in a circuit depth of  $\mathcal{O}(n^2+nt)$ , which due to the qubit-scaling procedure already discussed is bounded by  $\mathcal{O}(n^2)$ . Alternatively, Draper *et al.* present an adder requiring  $\mathcal{O}(n)$  ancilla qubits, and scaling with  $\mathcal{O}(\log n)$  circuit depth, without the need to enter the Fourier space, enabling our algorithm to scale with  $\mathcal{O}(n \log n)$  circuit depth, if  $\mathcal{O}(n)$  ancilla qubits are available [32].

## 7. The Adder Gate

The circuit implementation of the +d gate is shown in Figure 7. The general form of the +d gate, with d being an integer, is  $\bigotimes_{k=1}^n U1(2\pi d/2^k)$ , where n is the number of qubits in the main register [33]. Moreover, as our adder gates are conditioned on the state of the ancillary qubit, the general form of the controlled adder gate  $A_j^{+d}$  is given by,

$$A_j^{+d} = \prod_{k=1}^n U1_j^k (2\pi \frac{d}{2^k}),$$

where a  $U1_a^b$  gate is a U1 gate with a control on qubit a, a target on qubit b, and identity on all other qubits. Moreover, a U1 gate is defined as follows,

$$U1(\lambda) = \begin{pmatrix} 1 & 0 \\ 0 & e^{i\lambda} \end{pmatrix},$$

and is equivalent to an  $R_z(\lambda)$  gate up to a global phase of  $e^{i\frac{\lambda}{2}}$ , as defined by Barenco *et al.* in 1995 [34]. The circuit for  $A_i^{+d}$  is shown in Figure 8. For a more comprehensive discussion of the adder gate, see SI 8.

#### 8. The General Adder Gate

Let  $x \in \{0,1\}^n$ . When applying the QFT to such a binary-labelled standard basis vector, we obtain:

$$\frac{1}{2^{n/2}} \bigotimes_{l=0}^{n-1} (|0\rangle + e^{2\pi i x \frac{2^l}{2^n}} |1\rangle).$$

Thus, the action of the +1 gate is given by:

$$\frac{1}{2^{n/2}} \bigotimes_{l=1}^{n} U1(2\pi i \frac{2^{l}}{2^{n}})(|0\rangle + e^{2\pi i x \frac{2^{l}}{2^{n}}})|1\rangle$$

$$= \frac{1}{2^{n/2}} \bigotimes_{l=1}^{n} \left[ |0\rangle + \exp\left(2\pi i (x+1) \frac{2^{l}}{2^{n}}\right)|1\rangle \right].$$

A subsequent application of the inverse QFT would yield the desired state of  $|x+1\rangle$ . Note that multiple adder gates may be chained together while in the amplitude space, meaning that only one QFT would be required at the start of the circuit, and only one inverse QFT is requried at the end of the circuit. It is also worth noting that the periodicity of the imaginary exponential implies that this addition is actually addition modulo  $2^n$ , and so our  $\mathcal{H}$  operation encounters a boundary condition when there are non-zero amplitude states  $|x=0\rangle$  or  $|x=2^n\rangle$  (in practice, the boundary condition only becomes significant when the amplitudes of these extreme states are much greater than zero). However, it would not be expected for any algorithm to be able to circumvent this limitation, as it is intrinsic to the finite quantum mechanical system. Finally we can model a  $A^{+k}$  gate (adder +k) as follows,

$$A^{+k} = \bigotimes_{l=1}^{n} U1(2\pi i \frac{2^{l}}{2^{n}} k).$$

## 9. Efficient Scaling Through Qubit Addition

As discussed, if we wish to execute  $\mathcal{H}^t$  on the quantum processor, naively we would expect that to obtain a given variance we require a number of applications of  $\mathcal{H}$  that grow exponentially in the number of qubits

$$|q
angle_n:$$
  $-U1(rac{2\pi d}{2^1})$   $q_2:$   $U1(rac{2\pi d}{2^2})$   $\vdots$   $\vdots$   $\vdots$   $U1(rac{2\pi d}{2^n})$   $U1(rac{2\pi d}{2^n})$   $\vdots$   $\vdots$   $\vdots$   $\vdots$   $U1(rac{2\pi d}{2^n})$   $\vdots$   $\vdots$   $U1(rac{2\pi d}{2^n})$   $\vdots$   $\vdots$   $U1(rac{2\pi d}{2^n})$ 

FIG. 7. Quantum circuit implementing the Fourier space adder gate +d.

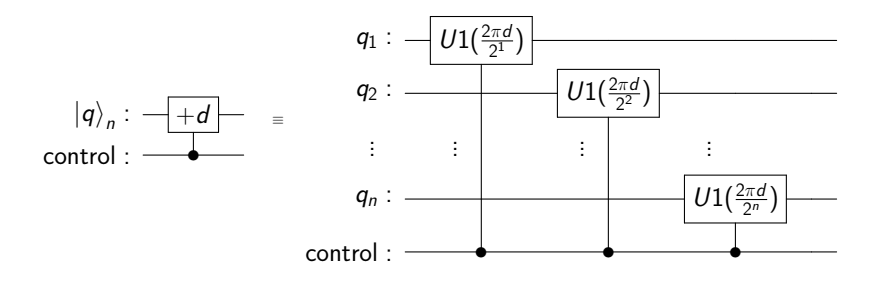


FIG. 8. Quantum circuit implementing the Fourier space controlled adder gate  $A_{\text{control}}^{+d}$ .

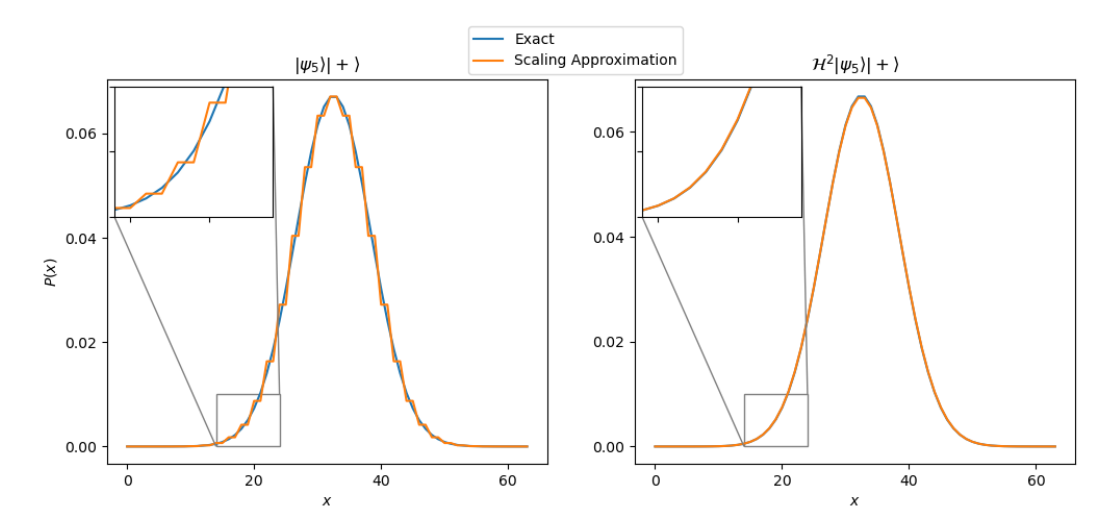


FIG. 9. Demonstration of Correction Iterations in the Efficient Scaling Procedure. Two Gaussians generated by the algorithm on 6 qubits are shown. The scaling approximation curve in the left panel is obtained with  $t_1 = 70$  and  $t_2 = 0$ , meaning that no correction iterations are performed after the scaling qubit is added to the least significant bit. The scaling approximation curve in the right panel is obtained with  $t_1 = 70$  and  $t_2 = 2$ , meaning that two correction iterations are applied after the scaling qubit is added. In both panels, the exact curve is generated by applying  $t_{\rm eff}$  iterations on *only* the final qubit count (meaning that the scaling procedure is not used), where  $t_{\rm eff} = 281$  in the panel on the left, and  $t_{\rm eff} = 283$  in the panel on the right.

in the final quantum register,  $n_m$ , in accordance with Equation 2. However, instead of performing all titerations in the space of  $n_m$  qubits, we can produce a distribution with the same variance  $\hat{\sigma}^2$  on a small, constant number of qubits. In doing so, we essentially produce a "low-resolution" version of the distribution that has the overall correct shape of the final distribution. We subsequently add a qubit in the  $|+\rangle$  state to the least significant qubit, apply a number of correction iterations implemented directly as the  $\mathcal{H}$  operator, and repeat this addition and iteration procedure  $n_m - n_1$  times. To understand how applying  $\mathcal{H}$  some number of times increases the resolution of the distribution after adding the  $|+\rangle$  qubit, it is important to better understand the distribution obtained after the addition. Figure 9 demonstrates both the distribution obtained immediately after adding a qubit in the  $|+\rangle$  state (in the panel on the left), and the distribution obtained after adding a qubit in the  $|+\rangle$  state followed by performing two correction iterations (directly implemented as applications of  $\mathcal{H}$ ). As expected, by virtue of mapping the amplitude of state  $|x\rangle$  to states  $|2x\rangle$  and  $|2x+1\rangle$ , each pair of two states shown in the figure have the same amplitude, resulting in the step-pattern shown. The panel on the right illustrates that it only takes two correction iterations to almost perfectly match the exact distribution. This is consistent with the theory discussed shortly. Moreover, while not shown in the figure, applying a couple more correction iterations would make the scaling approximation and exact distributions completely indistinguishable.

First, we define the i-qubit grid as,  $\{X_i\}$ . Then, the grid on i+1-qubits (obtained simply by adding a

qubit in the  $|+\rangle$  state) is given by,  $\{2X_i, 2X_i + 1\}$ . Allow the *i*-qubit mean to given by  $\mu_i$ . Upon doubling the number of qubits (with adjacent even and odd states sharing their amplitudes), the mean becomes  $\mu_{i+1} = 2\mu_i + 0.5$ . From the definition of variance, we have

$$\sigma_i^2 = \sum_{x \in X_i} (x - \mu_i)^2 P(x).$$

Thus we can compute the variance of the resulting distribution with,

$$\begin{split} \sigma_{i+1}^2 &= \sum_{x \in X_{i+1}} (x - \mu_{i+1})^2 P(x) \\ &= \frac{1}{2} \left( \sum_{x \in X_i} (2x - \mu_{i+1})^2 P(x) + \sum_{x \in X_i} (2x + 1 - \mu_{i+1})^2 P(x) \right) \\ &= \frac{1}{2} \sum_{x \in X_i} \left[ (2x - 2\mu_i - 0.5)^2 + (2x - 2\mu_i + 0.5)^2 \right] P(x) \\ &= \sum_{x \in X_i} \left[ 4(x - \mu_i)^2 + 0.5^2 \right] P(x) \\ &= 4 \left[ \sum_{x \in X_i} (x - \mu_i)^2 P(x) \right] + 0.5^2, \end{split}$$

Therefore,

$$\sigma_{i+1}^2 = 4\sigma_i^2 + 0.25. \tag{3}$$

Moreover, define  $t_i$  to be the number of iterations performed on  $n_i$  qubits, with  $n_1 \leq n_i \leq n_m$ , and let  $|\psi_i\rangle$  be the state obtained on  $n_i$  qubits after  $t_i$  iterations have been performed. Thus, assuming that  $\mathcal{H}$  is acting on the appropriately sized quantum system  $|\psi_{i+1}\rangle$  and  $|\psi_i\rangle$  are related as follows,

$$|\psi_{i+1}\rangle = \mathcal{H}^{t_{i+1}} |\psi_i\rangle |+\rangle.$$

Moreover, the variance of the distribution represented by  $|\psi_i\rangle|+\rangle$  is stated in Equation 3. First, the grid on  $n_i$  qubits is constant, given by  $\{X_i\}$ . Before applying  $\mathcal{H}$ , our distribution is simply over  $\{X_i\}$ , with a mean and variance given by

$$\mu_i = \sum_{x \in X_i} x P(x), \ \sigma_i^2 = \sum_{x \in X_i} (x - \mu_i)^2 P(x).$$

Upon applying  $\mathcal{H}$ , we obtain two distributions, one equal to the original distribution, and one equal to the original distribution shifted by one state to the right. The probability mass function of the new distribution would therefore be given by,

$$F(x) = pP(x-1) + (1-p)P(x).$$

Therefore, the mean of the new distribution would be given by,

$$\mu_i' = \sum_{x \in X} xpP(x-1) + x(1-p)P(x) = p(\mu_i + 1) + (1-p)\mu_i = p + \mu_i,$$

and the variance would be given by,

$$\begin{split} \sigma_i^{2\prime} &= \sum_{x \in X_i} (x - \mu_i')^2 F(x) \\ &= \sum_{x \in X_i} (x - \mu_i - p)^2 [pP(x - 1) + (1 - p)P(x)] \\ &= p \sum_{x \in X_i} (x - \mu_i)^2 P(x - 1) + (1 - p) \sum_{x \in X_i} (x - \mu_i)^2 P(x) \\ &+ \sum_{x \in X_i} [-2xp + 2\mu_i p + p^2] [pP(x - 1) + (1 - p)P(x)] \\ &= \sigma_i^2 + p \sum_{x \in X_i} P(x) - 2p \sum_{x \in X_i} pP(x) + \sum_{x \in X_i} p^2 P(x) \\ &= \sigma_i^2 + p(1 - p). \end{split}$$

Thus, the mean and variance on the  $n_i$  qubits corresponding to the distribution obtained after  $t_i$  iterations of  $\mathcal{H}$  are given by

$$\mu_i^{2\prime} = \mu_i + t_i p = 2\mu_{i-1} + 0.5 + t_i p, \tag{4}$$

$$\sigma_i^{2'} = \sigma_i^2 + t_i p(1-p) = 4\sigma_{i-1}^2 + 0.25 + t_i p(1-p).$$
 (5)

Or equivalently,

$$\mu_i^{2\prime} = 0.5 \times (2^{i-1} - 1) + \sum_{k=1}^{i} 2^{i-k} pt_k,$$

$$\sigma_i^{2\prime} = 0.25 \times \frac{4^{i-1} - 1}{3} + \sum_{k=1}^i 4^{i-k} p(1-p) t_k.$$

It is straight forward to use this equation to both compute the effective variance obtained after performing a number of iterations at various qubit counts, and to compute the iterations required at various qubit counts to obtain a given variance. It is important to emphasize that Equation 5 implies that the qubit scaling procedure incurs no additional error beyond that already incurred by the central limit theorem approximation to the normal distribution, as it allows for an arbitrary exact variance to be obtained. Intuitively, if you wish to obtain a distribution corresponding to t iterations performed on  $n_1$  qubits, if you first performed t iterations on the  $n_1$  qubits, and then performed some number of iterations on subsequent qubit counts, the total variance produced would exceed the desired variance. This expression describes how the number of iterations performed on the first qubit count may be reduced, and the number of removed iterations may then be translated to a number of correction iterations at higher qubit counts, allowing for the exact desired distribution to be obtained whilst still allowing for the correction iterations in the qubit scaling procedure to be made. Finally, Equation 5 shows that an arbitrary variance on n-qubits may be obtained while setting each  $t_i$  to essentially an arbitrary constant value, so long as  $t_1$  is set to give the desired variance on  $n_1$  qubits. As such, it is clear that this approach implies a total number of iterations scaling polynomially in the number of qubits to obtain an arbitrary variance.

#### 10. Resistance to Hardware Noise

The variant of the algorithm utilizing MCMR is also expected to be resistant to both bit-flip and, to a lesser extent, phase-flip errors by automatically discarding results in which such errors occur with high probability. The subsequent analysis assumes a simple noise model where errors in the execution of the

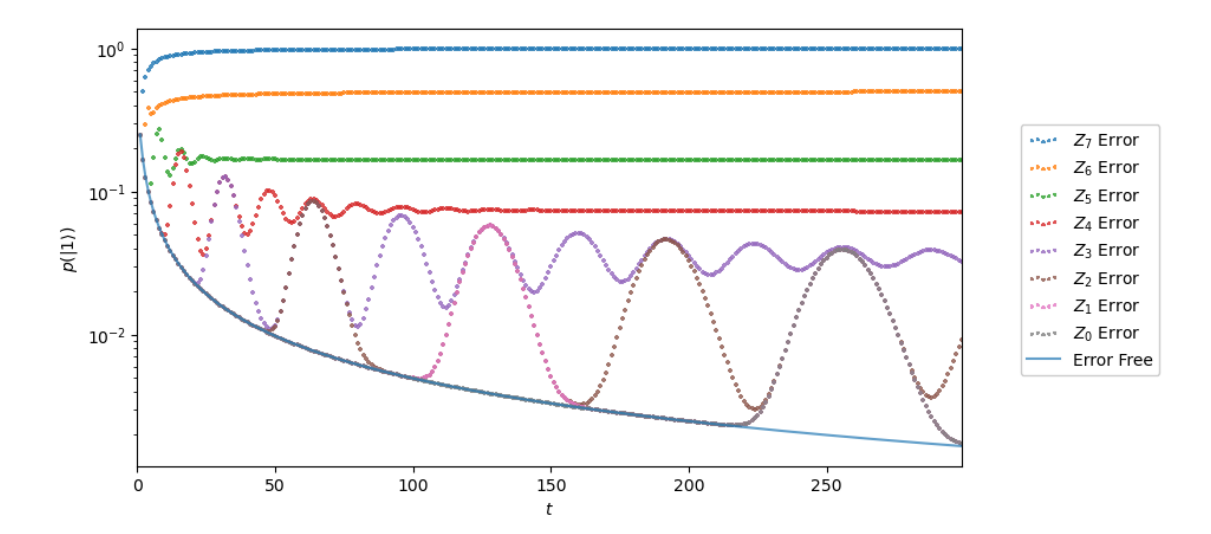


FIG. 10. 8 Qubit Demonstration of Rejection Probability as Function of Phase-Flip Errors. In this simulated experiment, the operator  $\mathcal{H}Z_j\mathcal{H}^t$  is applied to an initial state  $|0\rangle$ . The probability of measuring the  $|0\rangle$  ancillary state in the final application of  $\mathcal{H}$ , and thus the probability of rejecting a circuit execution in which an error occurred, is shown as  $p(|1\rangle)$ .

algorithm are dominated by the fidelity of two-qubit gate executions. Allow  $\epsilon$  to represent the two-qubit gate infidelity such that when executing any given two-qubit gate either a X or a Z gate (implementing a bit-flip and phase-flip error, respectively) gets subsequently randomly executed on either the control or target qubit. The probability of executing d such gates without obtaining any errors is therefore given by  $(1-\epsilon)^d$ .

For expository clarity, the following argument will concern itself with logical operations, such as mapping the state  $|x\rangle$  to  $|x+1\rangle$ , and we will not consider the Fourier basis entered by the QFT. Precisely, we will assume that the QFT and inverse QFT are applied in a noiseless channel, and that in-between these two operations the channel is subject to both phase-flip and bit-flip errors. As a result, a bit-flip error occurring in the hardware is experienced as a phase-flip error in the conceptual analytical space, and a phase-flip error on the hardware is similarly experienced as a bit-flip error in the conceptual space. This is similar to how a bit-flip error correcting code may be applied to correct a phase-flip error by applying a set of Hadamard transforms before and after the noisy channel.

Finally, we model the execution of a single iteration of  $\mathcal{H}$  as a single quantum gate, and so an error occurring in the execution of  $\mathcal{H}$  is modelled as one of  $Z_j$  or  $X_j$  being executed after  $\mathcal{H}$  with j selected uniformly at random. Note that here the notation  $A_j$  means gate A is executed on qubit j, and an identity gate is executed on all other qubits. Moreover, we assume that such errors occur with probability equal to the probability of any of the 2n CX gates implementing  $\mathcal{H}$  experiencing an error. Thus, the infideltity of the  $\mathcal{H}$  operation is given by  $1 - (1 - \epsilon)^{2n}$ . In the following analysis, we will use this model to examine the impact of the first occurrence of an error after t successful applications of  $\mathcal{H}$ . We will not examine the case where multiple errors occur in detail, but a similar argument holds in such cases nevertheless. We will now proceed by considering the two types of conceptual errors separately.

a. Analysis of Phase-Flip Errors We now assume that we are given an initial state  $|\psi_i\rangle$ , apply t iterations of  $\mathcal{H}$  to obtain some state  $\mathcal{H}^t |\psi_i\rangle$ , apply an error  $Z_j$  on some qubit with  $0 \leq j < n$ , and finally apply one last iteration of  $\mathcal{H}$ , giving the final state  $\mathcal{H}Z_j\mathcal{H}^t |\psi_i\rangle$ . Figure 10 shows the result of this experiment, showing the probability of measuring the  $|1\rangle$  ancillary state plotted for various j and t. As can be seen in this figure, the occurrence of any error strictly increases the probability of measuring the  $|1\rangle$  ancillary state, and thus of discarding the obtained error-affected result in post selection. We will now provide a general analysis of this type of error, and use the analysis to explain the plotted figure in greater detail. First, we define two new operators,  $A_m = Z \otimes I \otimes ... \otimes I$ , where there are m-1 identity gates and one Z gate, and  $B_k = I \otimes ... \otimes I$  where there are k identity gates, and such that k+m=n. We may then write,

$$Z_j = B_j \otimes A_{n-j},$$

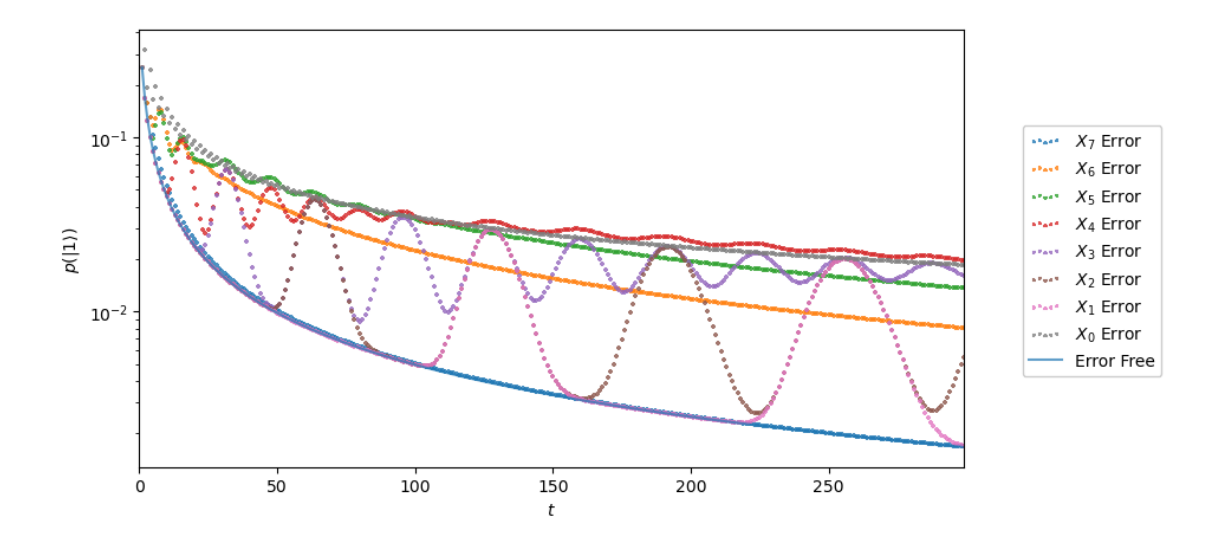


FIG. 11. 8 Qubit Demonstration of Rejection Probability as Function of Bit-Flip Errors. In this simulated experiment, the operator  $\mathcal{H}X_j\mathcal{H}^t$  is applied to an initial state  $|0\rangle$ . The probability of measuring the  $|0\rangle$  ancillary state in the final application of  $\mathcal{H}$ , and thus the probability of rejecting a circuit execution in which an error occurred, is shown as  $p(|1\rangle)$ .

where we implicitly assume that  $B_0 \otimes A_n = A_n$ , and that  $m \ge 1$ , as there must be at least one Z gate in the  $Z_j$  operator. First, we observe that  $A_m = \operatorname{diag}(1\ 1\ \dots\ -1\ -1)$ , where there are  $2^{m-1}$  consecutive +1 elements from the start, followed by  $2^{m-1}$  elements with value -1. Furthermore,  $B_j = \operatorname{diag}(1\ 1\ \dots\ 1)$  where there are  $2^j$  elements with value +1. By definition of the tensor product,  $B_j \otimes A_{n-1}$  thus represents a diagonal sign pattern consisting of  $2^{j}$  repetitions of the pattern given by  $A_{m}$  – meaning that the period of the pattern is  $2^m$ . For example, in the extreme cases,  $Z_0 = A_n$  represents a  $2^n \times 2^n$  diagonal matrix where the first half of the diagonal terms are all 1 and the second half of the diagonal terms are all -1 (thus having a period of  $2^n$ ), and  $Z_{n-1}$  represents a  $2^n \times 2^n$  diagonal matrix with the pattern diag (1-1) repeated  $2^{n-1}$  times. It is clear that the application of  $Z_j$  to a state  $\mathcal{H}^t | \psi_i \rangle$  will introduce a discontinuity to the wave function (beyond the negligible discontinuity already imposed by the discretization) at each pair of states x, x + 1 for which  $\operatorname{sign}(\langle x|Z_j|x\rangle) \neq \operatorname{sign}(\langle x+1|Z_j|x+1\rangle)$ . In particular, there is one such sign change in each pattern given by the diagonal of  $A_{n-j}$ , and so there are a maximum of  $2^{j}$  possible discontinuities introduced by  $Z_{j}$ . Moreover, after t iterations according to  $\mathcal{H}$ , only states  $|0\rangle$  through  $|t-1\rangle$  will have non-zero amplitudes, and so the number of discontinuities introduced by  $Z_j$  is given by  $\lfloor \frac{t}{2^{n-j}} \rfloor$ . This may be made more clear by considering an example. After the application of  $Z_j$  a possible state associated with the  $|0\rangle$  ancillary state may look like  $|\psi\rangle = |x\rangle - 2|x+1\rangle + |x+2\rangle$ , and so  $|\psi\rangle - |\psi+1\rangle = |x\rangle - 3|x+1\rangle + 3|x+2\rangle - |x+3\rangle$ , as opposed to the error free state of  $|x\rangle + |x+1\rangle - |x+2\rangle - |x-3\rangle$ , clearly illustrating how the sign-flip error leaves greater amplitude on the  $|1\rangle$  state because of the shift discontinuous negated distribution. Indeed, SI 12, shows that the cancellation property of the  $|1\rangle$  ancilla state only holds if the wave function is continuous. This analysis well explains the data shown in Figure 10. Of note, as j increases, as predicted by the increase in the number of discontinuities introduced, the probability of measuring the  $|1\rangle$  ancillary state increases, up to a near-1 probability of discarding the execution when a  $Z_7$  error occurs (in an 8-qubit system, numbered [0,7]). Furthermore, when the period of the error operator's sign pattern is greater than t (in particular, when it is greater than the number of states with amplitude >> 0) the action of  $Z_i$  is that of identity and so no error is incurred, hence why each of the  $Z_j$  curves follows the error-free curve for some number of t. For example, this explains why the  $Z_0$  operator follows the error-free curve until  $t \approx 220$  (observing that

Moreover, by applying the normal approximation for the distribution produced by t iterations of  $\mathcal{H}$ , it would be straight-forward to continue this analysis and obtain a closed-form expression for the probability of measuring the  $|1\rangle$  state after experiencing a  $Z_j$  error.

b. Analysis of Bit-Flip Errors The analysis for conceptual bit-flip errors follows a similar argument as that presented for the conceptual phase-flip errors, only with a couple small differences. Primarily, the discontinuities introduced by inserting an  $X_i$  operator come from swapping the amplitudes of two states

 $|x_0 \dots x_j \dots x_{n-1}\rangle$  and  $|x_0 \dots \overline{x}_j \dots x_{n-1}\rangle$ . As such, as j increases X is applied to less-and-less significant qubits, meaning that the distance between swapped states decreases exponentially. As a result, we would expect the error introduced by the  $X_j$  operator to increase as j decreases, and thus for the probability of measuring the  $|1\rangle$  ancillary state to increase as j decreases. In the extreme, for large n, the distribution given by  $\mathcal{H}^t |\psi_i\rangle$  is essentially continuous, and so swapping the amplitude on states  $|x\rangle$  and  $|x+\delta\rangle$  is essentially equivalent to an identity transformation, hence why the  $X_7$  operator is identical to the error-free line in Figure 11. The fact that  $X_j$  introduces more subtle discontinuities than  $Z_j$  is also reflected in Figure 11, noting that the probability of measuring the  $|1\rangle$  ancillary state (and thus of discarding a result in which an error occurred) is, in general, less than the corresponding probability for the  $Z_j$  operator. We expect that an expression for the net cancellation incurred for a given  $X_j$  and t may be obtained by following the preceding analysis.

## 11. Asymptotic analysis on the expected number of trials

In this section we analytically derive the expected number of trials to successfully load the desired distribution into a quantum register.

#### a. Without qubit scaling

First we look at the case where we do not perform qubit scaling in the state generation process. Suppose that we have a n-qubit quantum register originally in the computational basis state  $|x_0\rangle$ , where  $x_0$  is an integer in the range of  $[0, 2^n - 1]$ . Assume that  $x_0 + t < 2^n$ , after t - 1 iterations of  $\mathcal{H}$  on the quantum register, the state becomes

$$\mathcal{H}^{t-1} |x_0\rangle = \frac{1}{\sqrt{c_{t-1}}} \sum_{k=0}^{t-1} {t-1 \choose k} |x_0 + k\rangle,$$

where

$$c_{t-1} = \sum_{k=0}^{t-1} {t-1 \choose k}^2$$

is the normalization factor. On the next iteration, the state we have before measuring the ancilla qubit is

$$\frac{1}{2c_{t-1}} \sum_{k=0}^{t-1} \left[ \binom{t-1}{k} | x_0 + k \rangle + \binom{t}{k} | x_0 + k + 1 \rangle \right] | 0 \rangle + \frac{1}{2c_{t-1}} \sum_{k=0}^{t-1} \left[ \binom{t-1}{k} | x_0 + k \rangle - \binom{t}{k} | x_0 + k + 1 \rangle \right] | 1 \rangle$$

$$= \frac{1}{2c_{t-1}} \sum_{k=0}^{t} \binom{t}{k} | x_0 + k \rangle | 0 \rangle + \frac{1}{2c_{t-1}} \sum_{k=0}^{t-1} \left[ \binom{t-1}{k} | x_0 + k \rangle - \binom{t}{k} | x_0 + k + 1 \rangle \right] | 1 \rangle$$

The probability of measuring  $|0\rangle$  in the ancilla qubit is

$$P_t(|0\rangle) = \frac{1}{4c_{t-1}^2} \sum_{k=0}^t {t \choose k}^2 = \frac{c_t^2}{4c_{t-1}^2}$$

Using the Chu-Vandermonde identity, we have

$$c_t^2 = \sum_{k=0}^t {t \choose k} {t \choose k} = {2t \choose t}.$$

Therefore,

$$P_t(|0\rangle) = \frac{\binom{2t}{t}}{4\binom{2t-2}{t-1}} = 1 - \frac{1}{2t}.$$
 (6)

Consequently, the probability of getting a successful state with t applications of  $\mathcal{H}$  is

$$p_s(t) = \prod_{k=1}^{t} \left( 1 - \frac{1}{2k} \right), \tag{7}$$

and the expected number of trials to get one successful run with t iterations is given by the inverse of  $p_s(t)$ , i.e.

$$E_t[T] = \frac{1}{p_s(t)} = \frac{1}{\prod_{k=1}^t \left(1 - \frac{1}{2k}\right)}.$$

We take the logarithm of  $E_t[T]$  and expand the additive terms into Taylor series at  $\infty$ ,

$$\log(\mathbf{E}_t[T]) = -\sum_{k=1}^t \log\left(1 - \frac{1}{2k}\right)$$
$$= \sum_{k=1}^t \left(\frac{1}{2k} + O\left(\frac{1}{k^2}, k \to \infty\right)\right)$$
$$= \frac{1}{2} \sum_{k=1}^t \frac{1}{k} + O(1, t \to \infty).$$

The last equality holds because the series of the inverse squares and higher order powers converge absolutely. Then with the asymptotic development of harmonic series, we have

$$\log(\mathbf{E}_t[T]) = \frac{1}{2}\log(t) + O(1, t \to \infty).$$

Therefore, we have

$$E_t[T] = C\sqrt{t}(1 + O(1, t \to \infty)).$$
 (8)

We will now consider an upper bound, as for any x > -1,  $\log(1+x) \ge \frac{x}{1+x}$ . In our case,  $\log\left(1-\frac{1}{2k}\right) \ge \frac{-1}{2k-1}$  Thus,

$$\log(\mathbf{E}_{t}[T]) = -\sum_{k=1}^{t} \log\left(1 - \frac{1}{2k}\right)$$

$$\leq \sum_{k=1}^{t} \frac{1}{2k - 1}$$

$$= 1 + \sum_{k=1}^{t-1} \frac{1}{2k + 1}$$

$$\leq 1 + \sum_{k=1}^{t-1} \frac{1}{2k}$$

Using the upper bound of the harmonic series,

$$\log(\mathrm{E}_t[T]) \le \frac{1}{2}\log(t-1) + \frac{3}{2}$$

Therefore,

$$\mathcal{E}_t[T] \le e^{\frac{3}{2}} \sqrt{t-1} \tag{9}$$

Therefore the number of expected trials to get a successful state after t applications of  $\mathcal{H}$  grows sub-linearly with t.

First we show that the addition of a qubit in the  $|+\rangle$  state on the least significant end decreases the probability of measuring the ancilla in the  $|1\rangle$  state in the subsequent application of  $\mathcal{H}$  by 1/2, thereby increasing the algorithm's overall probability of success. Let  $a_{n,t}(x)$  be the amplitude of the n qubit basis state  $|x\rangle_n$  after t applications of  $\mathcal{H}$ , i.e. the state in the n-qubit quantum register is

$$|\psi_t\rangle_n = \sum_{x=0}^t a_{n,t}(x) |x\rangle_n.$$
 (10)

Now we perform another application of  $\mathcal{H}$  less the measurement, and we arrive at the state

$$\frac{1}{2} \sum_{x=0}^{t} a_{n,t}(x) (|x\rangle_n + |x+1\rangle_n) |0\rangle + \frac{1}{2} \sum_{x=0}^{t} a_{n,t}(x) (|x\rangle_n - |x+1\rangle_n) |1\rangle,$$

therefore the probability of measuring  $|1\rangle$  in the ancilla qubit is

$$P_{t+1}(|1\rangle) = \frac{1}{4} \left\{ a_{n,t}^2(0) + a_{n,t}^2(t) + \sum_{x=0}^{t-1} \left[ a_{n,t}(x) - a_{n,t}(x+1) \right]^2 \right\}$$
(11)

On the other hand, adding a qubit in the  $|+\rangle$  state to Equation 10, we have

$$|\phi_t\rangle_{n+1} = \frac{1}{\sqrt{2}} \sum_{x=0}^t a_{n,t}(x) (|2x\rangle_{n+1} + |2x+1\rangle_{n+1}).$$

Now we perform another application of  $\mathcal{H}$  less the measurement on  $|\phi_t\rangle_{n+1}$ , and we arrive at the state

$$\frac{1}{2\sqrt{2}} \sum_{x=0}^{t} a_{n,t}(x) \left( |2x\rangle_{n+1} + 2 |2x+1\rangle_{n+1} + |2x+1\rangle_{n+2} \right) |0\rangle 
+ \frac{1}{2\sqrt{2}} \sum_{x=0}^{t} a_{n,t}(x) \left( |2x\rangle_{n+1} - |2x+2\rangle_{n+1} \right) |1\rangle,$$

therefore the probability of measuring  $|1\rangle$  in the ancilla qubit is

$$P'_{t+1}(|1\rangle) = \frac{1}{8} \left\{ a_{n,t}^2(0) + a_{n,t}^2(t) + \sum_{x=0}^{t-1} \left[ a_{n,t}(x) - a_{n,t}(x+1) \right]^2 \right\}.$$
 (12)

Comparing Equation 12 with Equation 11, we have

$$P'_{t+1}(|1\rangle) = \frac{1}{2} P_{t+1}(|1\rangle). \tag{13}$$

Therefore adding a qubit before applying  $\mathcal{H}$  in the  $|+\rangle$  state on the least significant end decreases the probability of measuring the ancilla in the  $|1\rangle$  state in the subsequent application of  $\mathcal{H}$  by 1/2.

We now derive the expected number of trials in the context of qubit scaling. Suppose that we start with  $n_1$  qubits, and gradually increase the number of qubits to  $n_m$  in m stages. The qubit count increases by 1 in each subsequent stage, and the number of applications of  $\mathcal{H}$  is given by  $t_1, t_2, \ldots, t_m$ , respectively. From the analysis in Equation 9 we know that  $t_1$  is determined by the scaled variance  $\hat{\sigma}$  of the target distribution, and  $t_2, \ldots, t_m$  are bounded by some constant number that is independent of the number of qubits in the final state. In other words, let  $t_{\text{max}} = \max t_r, r = 2, \ldots, m$ , then  $t_{\text{max}}$  is independent of  $n_m$ . With this setting, the probability of getting one successful state from the process described above would be

$$p_s = \prod_{r=1}^m p_{s,r}(t_r),$$

where  $p_{s,r}(t_r)$  is the probability of success during stage r. From Equation 7 we have

$$p_{s,1}(t_1) = \prod_{k=1}^{t_1} \left( 1 - \frac{1}{2k} \right). \tag{14}$$

On the other hand, Equation 13 indicates that

$$p_{s,r}(t_r) > P_{r,1}(|0\rangle)^{t_r}$$

$$= \left[1 - \frac{1}{2}P_{r-1,t_{r-1}+1}(|1\rangle)\right]^{t_r}$$

$$\geq \left[1 - \frac{1}{2^{r-1}}P_{1,t_1+1}(|1\rangle)\right]^{t_r}$$

$$= \left[1 - \frac{1}{2^{r-1}}\frac{1}{2t_1}\right]^{t_r}$$

$$\geq \left[1 - \frac{1}{t_1}\frac{1}{2^r}\right]^{t_{\text{max}}},$$
(15)

where  $P_{r,k}(|0\rangle)$  and  $P_{r,k}(|1\rangle)$  are the probabilities of measuring  $|0\rangle$  and  $|1\rangle$  in the ancilla qubit after the k-th application of  $\mathcal{H}$  in stage r. Substituting Equation 15 into Equation 11 b, we have

$$\begin{split} p_{s} > & p_{s,1}(t_{1}) \prod_{r=2}^{m} \left[ 1 - \frac{1}{t_{1}} \frac{1}{2^{r}} \right]^{t_{\text{max}}} \\ = & p_{s,1}(t_{1}) \left( 1 - \frac{1}{2t_{1}} \right)^{-t_{\text{max}}} \prod_{r=1}^{m} \left[ 1 - \frac{1}{t_{1}} \frac{1}{2^{r}} \right]^{t_{\text{max}}} \\ = & p_{s,1}(t_{1}) \left[ \frac{\left( \frac{1}{t_{1}}; \frac{1}{2} \right)_{m}}{1 - \frac{1}{2t_{1}}} \right]^{t_{\text{max}}} \\ > & p_{s,1}(t_{1}) \left[ \frac{\left( \frac{1}{t_{1}}; \frac{1}{2} \right)_{\infty}}{1 - \frac{1}{2t_{1}}} \right]^{t_{\text{max}}}, \end{split}$$

where  $(a;q)_n = \prod_{k=1}^n (1-aq^k)$  is the q-Pochhammer symbol. And the expected number of trials to get one successful state is

$$E[T] = \frac{1}{p_s} < \frac{1}{p_{s,1}(t_1)} \left[ \frac{1 - \frac{1}{2t_1}}{\left(\frac{1}{t_1}; \frac{1}{2}\right)_{\infty}} \right]^{t_{\text{max}}}.$$
 (16)

Without loss of generality, we may assume that  $t_1 \geq 2$ , therefore

$$p_s > p_{s,1}(t_1) \left[ \frac{\left(\frac{1}{2}; \frac{1}{2}\right)_{\infty}}{1 - \frac{1}{4}} \right]^{t_{\text{max}}} \approx 0.385^{t_{\text{max}}} p_{s,1}(t_1),$$

which is independent of  $n_m$ . Consequently, the expected number of trials to get one successful state would be

$$E[T] = \frac{1}{p_s} < \frac{1}{p_{s,1}(t_1)} \left[ \frac{3}{4\left(\frac{1}{2}; \frac{1}{2}\right)_{\infty}} \right]^{t_{\text{max}}} \approx \frac{2.597^{t_{\text{max}}}}{p_{s,1}(t_1)}.$$

Therefore we have proved that the expected number of trials to get one successful state is bounded by a number that is independent of the number of qubits in the final state.

Now we derive a lower bound for  $\left(\frac{1}{t_1}; \frac{1}{2}\right)_{\infty}$  in terms of  $t_1$ . To do that, we take the logarithm of the q-Pochhammer symbol, and expand each log term into Taylor series

$$\begin{split} \log\left(\frac{1}{t_1};\frac{1}{2}\right)_{\infty} &= \sum_{r=1}^{\infty} \log(1 - \frac{1}{t_1}\frac{1}{2^r}) \\ &= -\sum_{r=1}^{\infty} \left[\sum_{k=1}^{\infty} \frac{1}{k} \left(\frac{1}{t_1 2^r}\right)^k\right] \\ &= -\sum_{k=1}^{\infty} \frac{1}{k t_1^k} \left[\sum_{r=1}^{\infty} \left(\frac{1}{2^k}\right)^r\right] \\ &= -\sum_{k=1}^{\infty} \frac{1}{k t_1^k} \frac{1}{2^k - 1} \\ &= -\frac{1}{t_1} - \sum_{k=2}^{\infty} \frac{1}{k t_1^k} \frac{1}{2^k - 1} \\ &> -\frac{1}{t_1} - \sum_{k=2}^{\infty} \frac{1}{k t_1^k} \frac{1}{2^k - 2} \\ &= -\frac{1}{t_1} - \frac{1}{2t_1} \sum_{k=1}^{\infty} \frac{1}{k t_1^k} \frac{1}{2^k - 1} \\ &= -\frac{1}{t_1} - \frac{1}{2t_1} \log\left(\frac{1}{t_1}; \frac{1}{2}\right)_{\infty}. \end{split}$$

It immediately follows that

$$\log\left(\frac{1}{t_1}; \frac{1}{2}\right)_{\infty} > -\frac{2}{2t_1 - 1},$$

or equivalently,

$$\left(\frac{1}{t_1}; \frac{1}{2}\right)_{\infty} > e^{-\frac{2}{2t_1 - 1}}.$$
 (17)

Substituting Equation 17 back into Equation 16, we have

$$E[T] < \frac{1}{p_{s,1}(t_1)} \left[ \left( 1 - \frac{1}{2t_1} \right) e^{\frac{2}{2t_1 - 1}} \right]^{t_{\text{max}}}. \tag{18}$$

#### 12. General Proof of $|1\rangle$ Ancillary State Cancellation

Consider some probability amplitude function function  $f: \mathbb{R} \to \mathbb{R}$ , such that we obtain a superposition

$$(f(x)|x\rangle + f(x+\delta)|x+\delta\rangle)|0\rangle + (f(x)|x\rangle - f(x+\delta)|x+\delta\rangle)|1\rangle$$

where  $\delta$  is some small real value. The ratio of the amplitude on the  $|1\rangle$  ancillary state to the total amplitude on both ancillary states may then be written as,

$$\lim_{\delta \to 0} \frac{f(x) - f(x+\delta)}{f(x) + f(x+\delta) + f(x) - f(x+\delta)} = \lim_{\delta \to 0} \frac{f(x) - f(x+\delta)}{2f(x)} = \lim_{\delta \to 0} \left[ \frac{1}{2} - \frac{1}{2} \frac{f(x+\delta)}{f(x)} \right]. \tag{19}$$

Suppose that f is a continuous function, meaning that  $\lim_{\delta\to 0} f(x+\delta) = f(x)$ . Then, Equation 19 reduces to 0 and consequently the probability of measuring the  $|1\rangle$  state is 0 for a small shift  $\delta$  when f is a continuous function. Now suppose that f is not continuous at point x, thus  $\lim_{\delta\to 0} f(x+\delta) \neq f(x)$ , then Equation 19 does not necessarily simplify to zero. Indeed, it is straightforward to construct an example in which  $f(x+\delta)/f(x)$  can assume an arbitrarily large or small value (by defining f to be piece-wise with the left and right hand limits at x being different), and thus the probability of measuring the  $|1\rangle$  could be an arbitrary zero or non-zero constant.

## 13. Simulation Based Approaches: Imaginary Time Evolution

Another variant of the algorithm which was explored simulates  $e^{\mathcal{H}t}$  instead of  $\mathcal{H}^t$ , where  $\mathcal{H}|x\rangle = |x-1\rangle + |x+1\rangle$ . A number of interesting observations were made regarding simulating  $e^{\mathcal{H}t}$  as opposed to  $\mathcal{H}^t$ , with some distinct advantages and disadvantages noted.

a. The Need for Imaginary Time Evolution in Simulation-Based Approaches

Originally, we considered simulating the dynamics of  $\mathcal{H}$  in accordance with the Schrodinger equation,

$$|\psi(t)\rangle = e^{-i\mathcal{H}t} |\psi(0)\rangle.$$

Of course, if such a Hamiltonian  $\mathcal{H}$  could be efficiently decomposed into some basis set (such as the set of n-bit Pauli strings) such that  $\mathcal{H} = \sum_k t_k \mathcal{H}_k$  where each  $\mathcal{H}_k$  is an element of the basis set with associated weight  $t_k$ , then the time evolution under  $\mathcal{H}$  could be approximated by the Trotter-Suzuki decomposition [35],

$$e^{-i\mathcal{H}t} \approx \left(\prod_{k=1}^k e^{-i\tau_k \mathcal{H}_k}\right)^P$$

where  $\tau_k = \frac{t \cdot t_k}{P}$ . However, in taking the Taylor expansion of  $e^{-i\mathcal{H}t}$ , we obtain,

$$e^{-i\mathcal{H}t} = \sum_{k=0}^{\infty} \frac{(-i)^k t^k \mathcal{H}^k}{k!} = \sum_{k=0,4,\dots} \frac{t^k \mathcal{H}^k}{k!} - i \sum_{k=1,5,\dots} \frac{t^k \mathcal{H}^k}{k!} - \sum_{k=2,6,\dots} \frac{t^k \mathcal{H}^k}{k!} + i \sum_{k=3,7,\dots} \frac{t^k \mathcal{H}^k}{k!},$$

which corresponds to four sets of weighted sums of Binomial distributions, each of which is separated by differing phases. As a result, the states experience an undesirable interference pattern which causes a distribution that is not normal to be produced. As such, we would like to simulate the object  $e^{\mathcal{H}t}$ , as it is intuitively similar to simulating  $e^{-i\mathcal{H}t}$  and avoids the phase complications.  $e^{\mathcal{H}t}$  expands as

$$e^{\mathcal{H}t} = \sum_{k=0}^{\infty} \frac{t^k}{k!} \mathcal{H}^k, \tag{20}$$

and as such corresponds to an infinite sum of Binomial distributions (noting that each  $\mathcal{H}^k$  produces a particular Binomial distribution with weight  $\frac{t^k}{k!}$ ) which is itself an approximation to a normal distribution in accordance with the central limit theorem. In understanding how  $e^{\mathcal{H}t}$  appears to produce the same normal distribution as  $\mathcal{H}^t$ , understanding the value of k in terms of t for which the weights  $\frac{t^k}{k!}$  are maximum may be beneficial. Whilst a more rigorous analytical argument could likely be made by substituting the factorial with an equivalent-valued Gamma function, and then computing  $\frac{\partial}{\partial k} \frac{t^k}{k!} \approx \frac{\partial}{\partial k} \frac{t^k}{\Gamma(k+1)}$ , numerical simulation suggests that the coefficient is greatest when  $k \approx t$ . As a result, the term in Equation 20 for which k = t,  $\mathcal{H}^t$ , is also likely the term which contributes the most to the transformation produced by  $e^{\mathcal{H}t}$ , providing some explanation as to why  $\mathcal{H}^t$  appears to produce the same distributions as  $e^{\mathcal{H}t}$ . Of course, if  $\mathcal{H} = \mathcal{H}^{\dagger}$ , then  $e^{\mathcal{H}t}$  will not be unitary for  $t \in \mathbb{R}$ . Thus, we have motivated the need for imaginary time evolution in a simulation based approach.

# b. Imaginary Time Evolution

In 2017, Li and Benjamin presented a quantum-classical hybrid algorithm for the purpose of simulating the Shrodinger equation [36]. This approach assumes that the state of the wave function at time t,  $|\phi(t)\rangle$ , may be approximated by a parameterized trial wave function  $|\psi(t)\rangle \equiv |\psi(\vec{\theta}(t))\rangle$ , where  $\vec{\theta}(t)$  are a set of variational time-dependant parameters. In 2019, McArdle *et al.* expanded upon the aforementioned work to describe how this simulation procedure may be applied to the variational simulation of non-unitary objects such as  $e^{\mathcal{H}t}$ . In summary, the non-unitary trajectory of a given starting state is projected onto a unitary evolution through the parameters of the variational quantum circuit implementing the trial wave function.

As a result, a simulation based approach utilizing ITE for the presented distribution generating algorithm has a number of advantages and one significant challenge. The advantages are (1) the parameterized circuit captures degrees of freedom enabling shallower NISQ-friendly circuits to be obtained, (2) allows for continuous values of t (as opposed to the main approach presented which requires integer values for t), (3) the alternating even and odd state cancellation which motivated the redefinition of the Hamiltonian as  $\mathcal{H}|x\rangle = |x\rangle + |x+1\rangle$  is circumvented, allowing the original definition of  $\mathcal{H}|x\rangle = |x-1\rangle + |x+1\rangle$  to be directly used, and (4) the definition of the Hamiltonian could be modified to easily enable the creation of a potentially broad class of distributions. The main challenge in using the ITE approach is that it requires the creation of a variational circuit capturing the necessary degrees of freedom in its parameters. Moreover, it is necessary to do so without introducing an exponential number of parameters (and thus number of gates) so as to remain competitive with the primary Galton simulation approaches described in this work. As such, a variational circuit should be constructed which effectively captures knowledge of the problem at hand, but how to do so in this particular instance remains a problem for future investigation.